frontiers | Frontiers in Marine Science

TYPE Original Research
PUBLISHED 07 January 2025
DOI 10.3389/fmars.2024.1504821

OPEN ACCESS

EDITED BY
Xiaohui Xie,
Ministry of Natural Resources, China

REVIEWED BY
Yun Qiu,
State Oceanic Administration, China
Vijay Tallapragada,
NCEP Environmental Modeling Center (EMC), United States

*CORRESPONDENCE
Dongxiao Wang
dxwang@mail.sysu.edu.cn

RECEIVED 01 October 2024
ACCEPTED 21 November 2024
PUBLISHED 07 January 2025

CITATION
Le Z, Subrahmanyam MV, Raju PVS, Pathirana G, Wang D and Song W (2025) A revisit of the semi-geostrophic eddy east of the Sri Lanka dome with anisotropy insight. *Front. Mar. Sci.* 11:1504821. doi: 10.3389/fmars.2024.1504821

A revisit of the semi-geostrophic eddy east of the Sri Lanka dome with anisotropy insight

Zhou Le[1], M. V. Subrahmanyam[2], Pemmani Venkata Subba Raju[3], Gayan Pathirana[4], Dongxiao Wang[1,5]* and Wei Song[1]

[1]School of Marine Sciences, Sun Yat-sen University, Zhuhai, China, [2]School of Marine Sciences, Hainan Tropical Ocean University, Sanya, China, [3]Centre for Ocean-Atmospheric Science & Technology, Amity University Rajasthan, Jaipur, Rajasthan, India, [4]Department of Oceanography and Marine Geology, Faculty of Fisheries and Marine Sciences & Technology, University of Ruhuna, Matara, Sri Lanka, [5]Southern Marine Science and Engineering Guangdong Laboratory (Zhuhai), Zhuhai, China

During boreal summer, the Southwest Monsoon Current (SMC) turns northeastward, transporting highly saline water into the Bay of Bengal (BOB) and significantly influencing the dynamics of the upper ocean. Previous studies have shown that an anticyclonic semi-geostrophic (SG) eddy forms on the eastern flank of the SMC, this formation associated with the kinetic energy transfer via the barotropic instability (BTI). The presence of such an eddy can attenuate the meridional salinity flux, potentially affecting the development of the circulation within the BOB. Acknowledging the importance of this phenomenon, this study revisits the SG eddy using satellite altimetry data, reanalysis datasets and *in-situ* observations from the Research Moored Array for African-Asian-Australian Monsoon Analysis and Prediction (RAMA) project. Our results show that a cyclonic eddy-like (CE-like) negative Sea Level Anomaly (SLA), generated in the eastern BOB due to regional anomalous wind stress curl, also contributes to the formation of the SG eddy. During the formation, mean flows on the northern edge of the SG eddy are strengthened, while southeastward currents on the eastern edge are structured influenced by CE-like SLA. Further instability analyses indicate that the anisotropic component of BTI is significantly larger than the isotropic component, which is attributed to the weak nonlinear planetary geostrophic convergence of the SG eddy and the strong horizontal shear in mean flow field induced by CE-like SLA. Additionally, our results point out that anomalies in wind stress curl over the eastern BOB and subsequent formation of negative SLA are likely influenced by the Indian Ocean Dipole. These findings suggest that the coupling between SMC instability and regional wind stress curl may play a pivotal role in the generation of SG eddy on interannual timescale, with important implications for regional ocean dynamics.

KEYWORDS

Bay of Bengal, Southwest Monsoon Current, Semi-Geostrophic eddy, anisotropy, Indian Ocean Dipole

1 Introduction

The Bay of Bengal (BOB), a marginal basin in the northern Indian Ocean, is well known for its low salinity and productivity (Beal et al., 2020). Additionally, its circulation is strongly influenced by dynamic factors such as the Asian Monsoon (Schott and McCreary, 2001; Jinadasa et al., 2020). Researchers have increasingly focused on this basin in recent years (Qiu et al., 2019; Huang et al., 2021; Ding et al., 2023). However, the variability of oceanic circulation and wave/eddy activities has left many questions unresolved in the mouth region of the bay.

The spring Wyrtki (1973) jet excites an equatorial Kelvin wave, part of which propagates along the periphery of the bay as a coastal Kelvin wave. A Rossby wave radiated by this coastal Kelvin wave is observed south of Sri Lanka during the Southwest Monsoon (SM) season, due to the topographic "bump" near 5°N. Cheng et al. (2018) noted that a similar "bump" near 15°N in the central BOB also promotes the radiation of Rossby waves from the eastern boundary. The arrival of this Rossby wave causes the northward migration of the Southwest Monsoon Current (SMC) and the disappearance of westward flow south of Sri Lanka (Schott et al., 1994). Chen et al. (2017) argued that equatorial waves substantially modulate currents in the tropical Indian Ocean. They illustrated that eddy-like Sea Surface Height anomalies near 5°N are predominantly manifestations of symmetric Rossby waves, primarily induced by intraseasonal wind stress forcing within the equatorial waveguide and the reflection of equatorial Kelvin waves at the eastern boundary. Their research emphasizes the disturbances in the flow field of lower latitude regions orginate from equatorial remote forcing.

Vinayachandran and Yamagata (1998) pointed out that during the SM season, a thermal dome and an anticyclonic vortex/eddy occur on the east side of Sri Lanka (near 8°N). The thermal dome, also known as the Sri Lanka Dome (SLD), and its seasonality and interannual variability has been discussed by Cullen and Shroyer (2019). Previous studies also indicate that during the SM season, the development of the SLD corresponds to Eddy Kinetic Energy (EKE) increment in the western coastal area of the BOB's mouth region (Burns et al., 2017; Pathirana et al., 2022). The anticyclonic eddy on the east side of SLD in shape with a radius of about 150 km, features at a smaller scale than the Rossby radius of deformation. Therefore, the anticyclonic eddy is certainly governed by the semi-geostrophic (SG) dynamics in an oceanic context (Badin, 2012). Vinayachandran and Yamagata (1998) argued this eddy is balanced by weak planetary wave dispersion and weakly nonlinear planetary geostrophic divergence, also satisfying the unique conditions of intermediate geostrophic dynamics discussed by Yamagata (1982) and Williams and Yamagata (1984): beta parameter $\beta^* < O(1)$, stratification parameter $s^* \sim S\beta^*$, and Rossby number $R^* \sim E(\beta^*)^2$, where S and E are numbers of $O(1)$. Energy analysis of the SG eddy reveals a direct conversion from Mean Kinetic Energy to EKE suggesting that Barotropic Instability (BTI) is the mechanism leading to eddy generation. Based on results from numerical model with coarse resolution, they also indicated that local wind stress curl anomalies over the eastern BOB have the potential to excite Rossby waves, which propagate westward and modulate the oceanic flow field along the 8°N zonal section. Today, the response of oceanic circulation and the formation of SG eddies can be more precisely illustrated using high-resolution data from the *In-situ* observations of Research Moored Array for African-Asian-Australian Monsoon Analysis and Prediction (RAMA) project, as well as nearly 30 years satellite altimetry data. This is one motivation for this study.

Numerous articles on eddy generation mechanisms have emphasized the importance of nonlinear terms. Cheng et al. (2018) investigated the role of nonlinearity in the eddy generation process using a reduced-gravity model, and indicated that the advection term dominates the wave-to-eddy transition among all nonlinear terms. Wang et al. (2021) also indicated that eddy generation requires nonlinear processes, as shown by modelling results. An advanced method for diagnosing oceanic internal instability with anisotropy insight can be applied to the analysis of nonlinear terms, as it further decomposes BTI into several distinct terms (Qiao et al., 2023). This method employed in this study is deemed well-suited for analyzing the generation process of the SG eddy.

The remainder of this paper is organized as follows: Section 2 introduces the datasets and methods utilized in this study. In Section 3, we first identify years with strong SG eddy signal, then analyze the correlation between their intensity and both the equatorial and local wind fields. Subsequently, we present several case studies on the formation of the SG eddy. Based on the evolution in the oceanic flow field, we conduct a detailed analysis of oceanic internal instability with anisotropy insight. Section 4 provides a summary and discussion of the findings.

2 Data and methods

2.1 Data

Sea Level Anomaly (SLA) data, available from the European Copernicus Marine Environment Monitoring Service (CMEMS), is produced based on satellite altimetry data. The daily dataset has a spatial resolution of 0.25° × 0.25°, and the period from January 1993 to December 2020 is used in this study. This study also utilizes products derived from satellite observations, including the Mesoscale Eddy Atlas provided by Archiving, Validation and Interpretation of Satellite Oceanographic data (AVISO+), and the Ocean Surface Currents Analyses Real-time (OSCAR) generated by Earth Space Research.

Surface wind velocity at 10 meters height is derived from the fifth generation ECMWF atmospheric reanalysis (ERA5), a widely used and recognized model output. The monthly data from January 1993 to December 2020, used in this study, has a spatial resolution of 0.25° × 0.25°.

Temperature and salinity data for the upper ocean (above 500 meters depth), used in this paper to illustrate the EKE budget are obtained from the Simple Ocean Data Assimilation ocean/sea ice reanalysis (SODA) v3.3.1 dataset with 5 days resolution. *In-situ* observation data from the RAMA buoy in 90°E, 8°N is also used.

2.2 Methods

2.2.1 EKE budget and oceanic internal instabilities

EKE is calculated using the formula $EKE = \frac{1}{2}(u'^2 + v'^2)$, where u' and v' represent the intraseasonal components of zonal and meridional velocity, respectively, obtained through a 30-90 days band-pass filter. The budget for key regions and specific period can be further diagnosed using the following equation (Ivchenko et al., 1997; Zu et al., 2013):

$$\partial(EKE)/\partial t = WW + PW + T4 + ADV + F$$

Here, $\partial(EKE)/\partial t$ represents the temporal variation of EKE, the contribution of wind stress work (WW) to the EKE per unit mass is defined as:

$$WW = \frac{1}{\rho_0}(u'\tau_x' + v'\tau_y')$$

The pressure work (PW) consists of the exchange between Eddy Potential Energy (EPE) and EKE and the pressure flux term through the boundary, and is defined as:

$$PW = -\frac{1}{\rho_0}\left(u'\frac{\partial p'}{\partial x'} + v'\frac{\partial p'}{\partial y}\right)$$

Here, p is the pressure, and the advection of EKE (ADV) is defined as:

$$ADV = -\left(u'\frac{\partial EKE}{\partial x} + v'\frac{\partial EKE}{\partial y}\right)$$

F represents the sum of horizontal friction, vertical friction, and bottom friction. However, these dissipation-related terms have not been calculated in this study and are regarded as the residual term in the energy balance equation.$T4$ represents Barotropic Instability, which signifies the energy conversion between Mean Kinetic Energy (MKE) and EKE. The growth of instability is led by the increased horizontal and vertical shears of the mean current. Besides, Baroclinic Instability (BCI) represents the energy conversion between Mean Potential Energy (MPE) and EPE. Following Chen et al. (2018), the definitions are:

$$BCI = -\frac{g}{\rho(\frac{\partial \overline{\rho_b}}{\partial z})}\left(\langle u'\rho'\rangle\frac{\partial\langle\rho\rangle}{\partial x} + \langle v'\rho'\rangle\frac{\partial\langle\rho\rangle}{\partial y}\right)$$

$$BTI = -\left(\langle u'u'\rangle\frac{\partial\langle u\rangle}{\partial x} + \langle u'v'\rangle(\frac{\partial\langle u\rangle}{\partial y} + \frac{\partial\langle v\rangle}{\partial x}) + \langle v'v'\rangle\frac{\partial\langle v\rangle}{\partial y}\right)$$

where $\rho_0 = 1025\ kg/m^3$ is the reference potential density, and $\overline{\rho_b}$ is a depth-dependent background density. $\rho' = \rho - \rho$; $u'(x,y,z,t) = u(x,y,z,y) - u(x,y,z,t)v'(x,y,z,t) = v(x,y,z,y) - v(x,y,z,t)$, where $\langle\cdot\rangle$ denotes the temporal mean of variable.

2.2.2 Lagrangian EKE

Ding et al. (2020) proposed a comprehensive concept, Lagrangian EKE (LEKE), as an additional metric. It combines gridded EKE calculated in the Eulerian framework with tracked coherent mesoscale eddies in the Lagrangian framework:

$$LEKE = \frac{\iint EKE \cdot \omega_x \cdot \omega_y \cdot dS}{\iint \omega_x \cdot \omega_y \cdot dS}$$

This calculation enables us to differentiate the EKE between cyclonic and anticyclonic eddies within the same region.

2.2.3 Anisotropy analysis

Corresponding to anisotropy decomposition, BTI can be separated into an isotropy production and an anisotropy production related to the mean-flow strain (Qiao et al., 2023):

$$BTI = -EKE \cdot div + (-L\ \cos\theta_a \cdot \overline{S_n} - L\ \sin\theta_a \cdot \overline{S_s})$$

The first term on the right-hand-side is isotrophy production, while the remaining terms represent anisotropy production. Where $div = \frac{\partial\bar{u}}{\partial x} + \frac{\partial\bar{v}}{\partial y}$ is the divergence of the mean flow, $S_n = \frac{\partial\bar{u}}{\partial x} - \frac{\partial\bar{v}}{\partial y}$ and $S_s = \frac{\partial\bar{u}}{\partial y} + \frac{\partial\bar{v}}{\partial x}$ are the normal (stretch) and shear rates of the mean flow strain, respectively. $L\ \cos\theta_a = \frac{\langle u'^2 - v'^2\rangle}{2}$; $L\ \sin\theta_a = \langle u'v'\rangle$, L represents the portion of EKE related to anisotrophy (Waterman and Lilly, 2015).

3 Results

3.1 Basic feature of SG eddy

Higher values of EKE are observed in the mouth region of BOB. On the eastern side, coastal trapped waves travel northward along the eastern boundary and radiate Rossby waves westward at the topographically bumped region. The arrival of these waves enhances the intraseasonal variability in the flow field, leading to larger EKE values on the eastern side near 6°N (as shown in Figure 1). However, under certain circumstances, a pronounced anticyclonic eddy can also form on the eastern side of SLD. Since the SG eddy may not be long-lived, it is not as prominently featured in the spatial pattern of EKE climatology as coastal regions.

Previous studies have indicated that 8°N serves as a pathway for westward propagating Rossby waves excited by local wind stress curl (Vinayachandran and Yamagata, 1998), which could promote the SG eddy formation. Therefore, the meridional current velocity (v) along 8° N, presented as a Longitude-Time diagram (also known as Hovmöller diagram) in Figure 2, reveals the potential signal of the SG eddy. In Figure 2C, negative v-velocity between 82°E and 84°E is paired with positive v-velocity between 84°E and 86°E from May to July, which signifies a cyclonic SLD in the coastal area and the northeastward SMC run into the central BOB. During the SM season (June, July, August and September), weak negative v-velocity is observed from the eastern edge of the SMC (87°E) to the eastern boundary of the BOB at 98°E. This pattern suggests a high likelihood of the anticyclonic SG eddy formation on the eastern flank of the SMC.

To identify a significantly developed SG eddy in the central area of the mouth region, we calculated the time series of LEKE, as shown in Figure 3. The time series of cyclonic eddy-related kinetic energy (CE-LEKE) stands for the SLD strength in the western coastal area, the anticyclonic eddy related kinetic energy (AE-

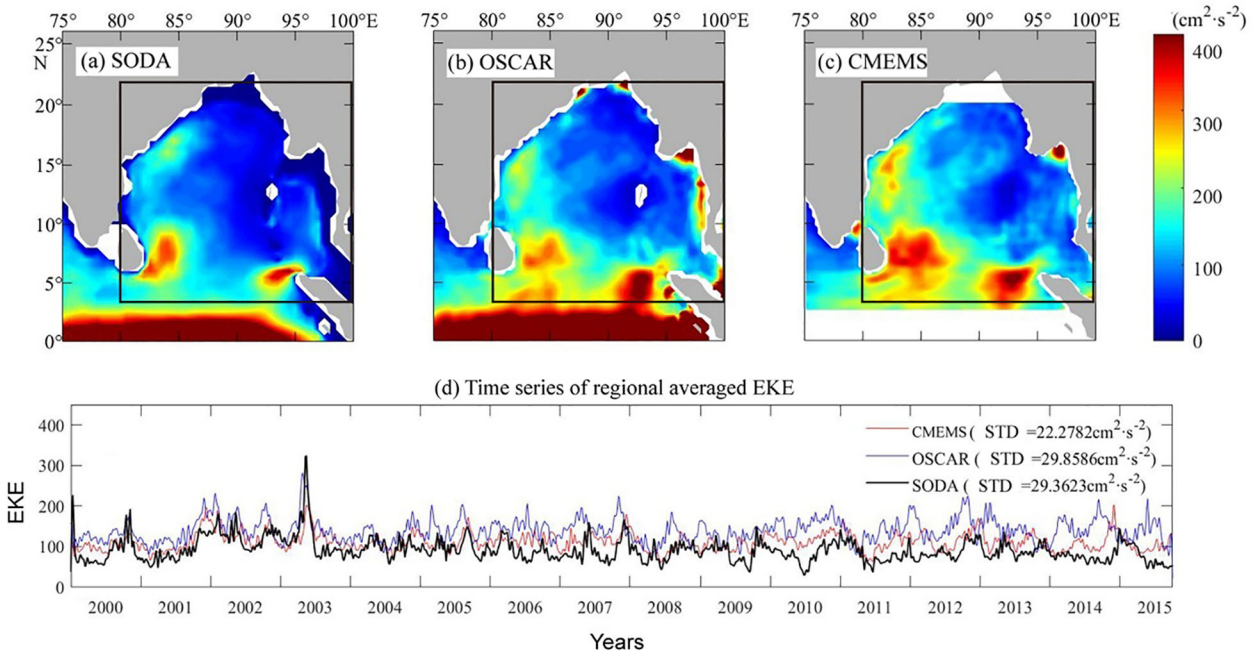

FIGURE 1
Spatial distribution of EKE in the BOB, averaged during the Southwest Monsoon season, calculated from **(A)** SODA currents, **(B)** OSCAR, and **(C)** CMEMS altimetry data derived currents. **(D)** The time series of EKE, averaged from 3°-22°N and 80°-100°E (indicated with black boxes in panels **(A–C)**). Figures 1A–D are reproduced from Le et al. (2020). STD means standard deviation.

LEKE) represents the strength of the SG eddy in the central area. The results indicate that the central area AE-LEKE value are notably larger than the western coastal area CE-LEKE value in several years, such as 2020, 2010, 1998 and 2006.

3.2 Correlation between local wind stress curl anomaly and the SG eddy formation

The upper ocean circulation at lower latitudes is significantly influenced by Rossby waves. We aim to investigate cases where Rossby waves excited by local wind stress curl anomaly during the SM season (June, July, August and September), lead to the generation of the SG eddy in the central area of the mouth region, especially when there is no significant anomaly in the equatorial wind field during the pre-SM season (March, April and May).

Figure 4 shows the anomaly of equatorial wind stress during the pre-SM season and wind stress curl over the eastern BOB during the SM season, covering years from 1993 to 2020. The data suggest that stronger AE-LEKE in the central area is associated with similar wind field anomaly: the equatorial wind field anomaly is not

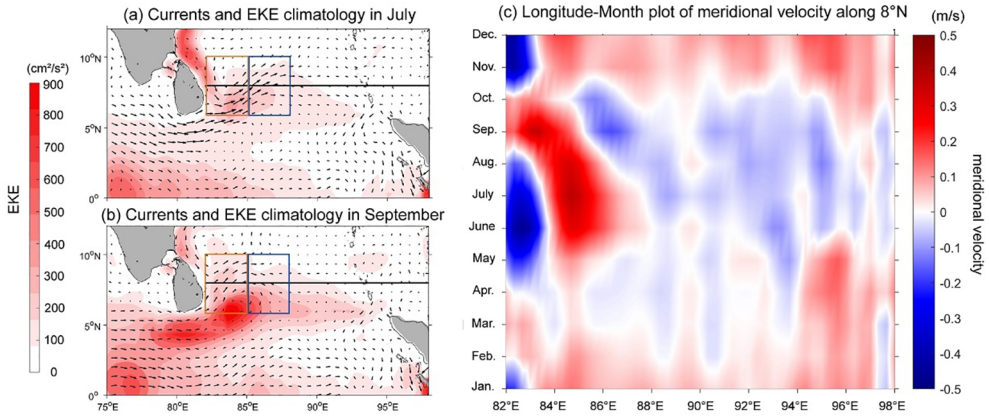

FIGURE 2
Surface currents (arrows) and EKE (color shading) in July **(A)** and September **(B)**. **(C)** Longitude (x axis) -Month (y axis) plot of the meridional current (v) along 8°N.

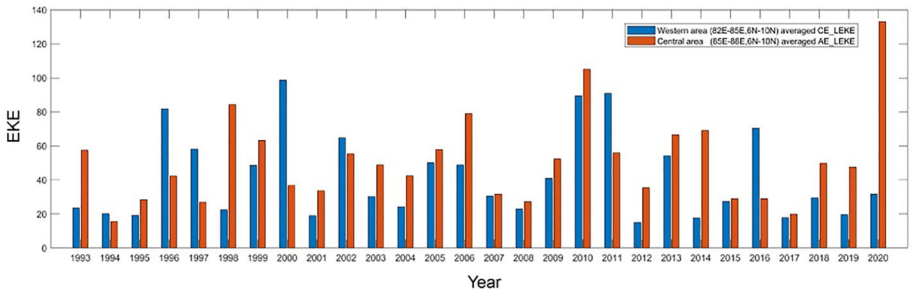

FIGURE 3
Time series of LEKE, from 1993 to 2020. Blue bars represent CE-LEKE, indicating the intensity of the SLD in the western area (82°E-85°E, 6°N-10°N, indicated with orange boxes in Figures 2A, B). Orange bars represent AE-LEKE, indicating the intensity of the SG eddy in the central area (85°E-88°E, 6°N-10°N, indicated with blue boxes in Figures 2A, B).

pronounced in pre-SM season, but the anticyclonic wind stress curl weakens during the SM season, as observed in 2020, 2010, and 1998. In other words, there is a strong cyclonic anomaly in the surface wind field over the eastern BOB. Figure 4B displays the tropical Indian Ocean Dipole (IOD) index, accessible on the National Climate Center's website. Notably, 2010 and 1998 were extreme/strong negative IOD years, while 2020 was a weak negative IOD year. Combining the information from Figures 3, 4, the classification of years when the SG eddy is notably greater than the SLD is summarized in Table 1.

Compared with climatology of sea surface wind over BOB during the SM season (as shown in Figure 5A), wind anomaly for negative IOD years (as identified in Figure 4B) are depicted in Figure 5B, pronounced cyclonic wind anomalies developed over the southern BOB, which are conducive to the development of negative SLA in the vicinity of SLD and positive SLA to the east of SLD (favoring the formation of the SG eddy). Furthermore, we composed the wind anomaly for the years with strong SG eddy signal (1998, 2010, 2020) and contrasted them with climatology in Figure 5C. A student-test at the 90% confidence level was used to

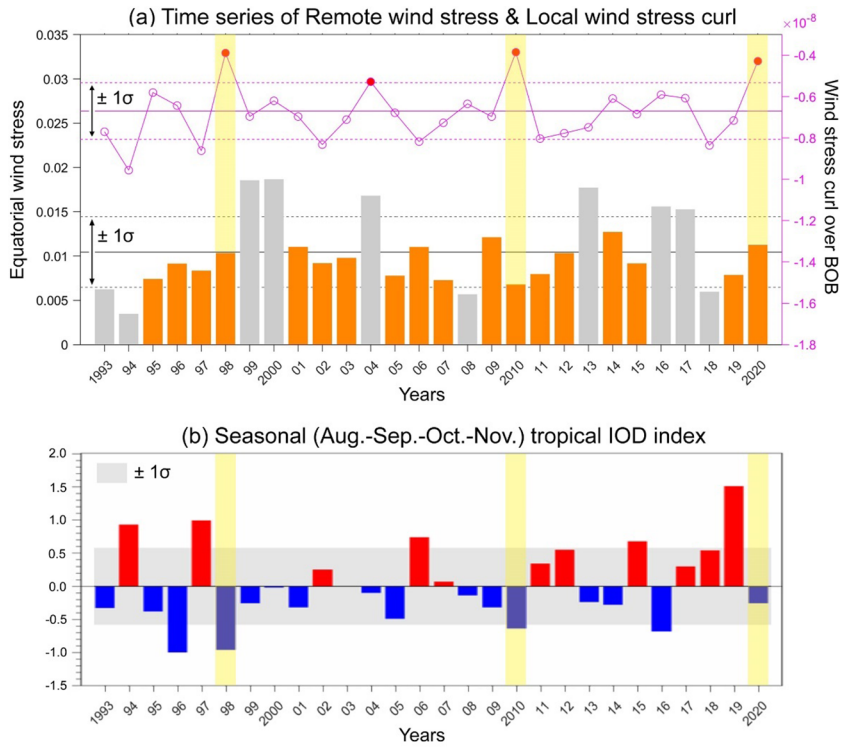

FIGURE 4
(A) Bars indicate interannual time series of equatorial (70°E-90°E, 3°S-3°N) wind stress during the pre-Southwest Monsoon season. The orange bars indicate values within one standard deviation of the climatological mean, while the gray bars represent values that exceed one standard deviation. Pink line with dots indicate interannual time series of wind stress curl over the eastern BOB (90°E-100°E, 5°N-10°N) during the Southwest Monsoon season. **(B)** Seasonal (tropical) IOD index provided by the National Climate Center.

10.3389/fmars.2024.1504821

TABLE 1 Classification of years when SG eddy is notably greater than SLD.

Years featured as the intensity of semi-geostrophic AE greater than CE	Conditions		Main forcing mechanism
	(1) Equatorial wind stress anomaly (positive)	(2) Local wind stress curl anomaly (positive)	
/	Yes	Yes	Both remote and local wind forcing.
1999, 2013	Yes	No	Remote wind forcing.
1998, 2010, 2020	No	Yes	Local wind forcing.
1993, 2006, 2014	No	No	Other forcing mechanisms

confirm that the discrepancy in the wind field between the composite and the climatology are significant in both zonal and meridional components. Result indicates the anomalous wind field primarily located in the eastern BOB north of 7°N, leading to the excitation of westward-propagating Rossby waves and promote the formation of SG eddy.

Figures 6–8 illustrate the formation process of the SG eddy in 1998, 2010 and 2020, respectively. The SMC is robust prior to the formation of the SG eddy, initiating northeastward flow on the western edge of the SG eddy (as shown in Figures 6A, 7A, 8A). Subsequently, the strengthening of negative SLA in the eastern area of mouth region promotes the development of southeastward flow

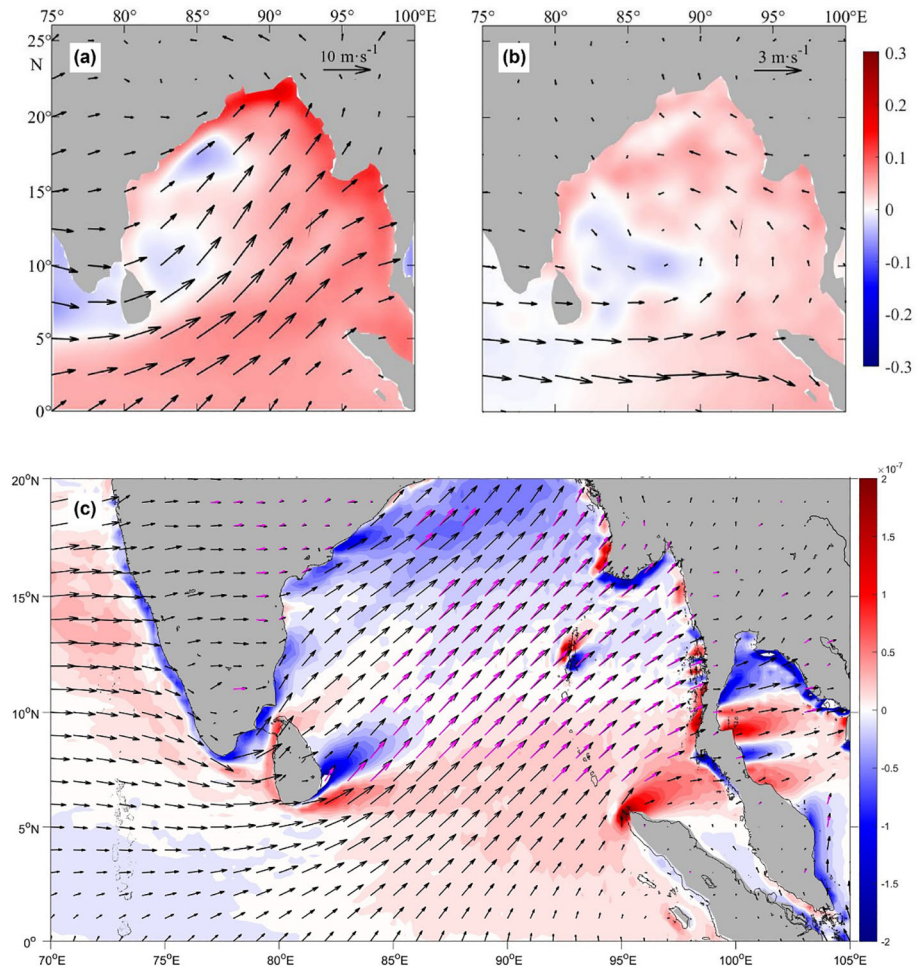

FIGURE 5
(A) Climatological-mean surface wind and **(B)** negative IOD years composite of wind anomaly (arrows) and sea level anomaly (color shading) averaged during SM season. Figures 5A, B are reproduced from Le et al. 2020. **(C)** Composite of surface wind stress (arrows) and wind stress curl (color shading) for the years 1998, 2010, 2020. Purple arrows indicate significant anomaly which have passed t-test at the 90% confidence level, compared to the climatology.

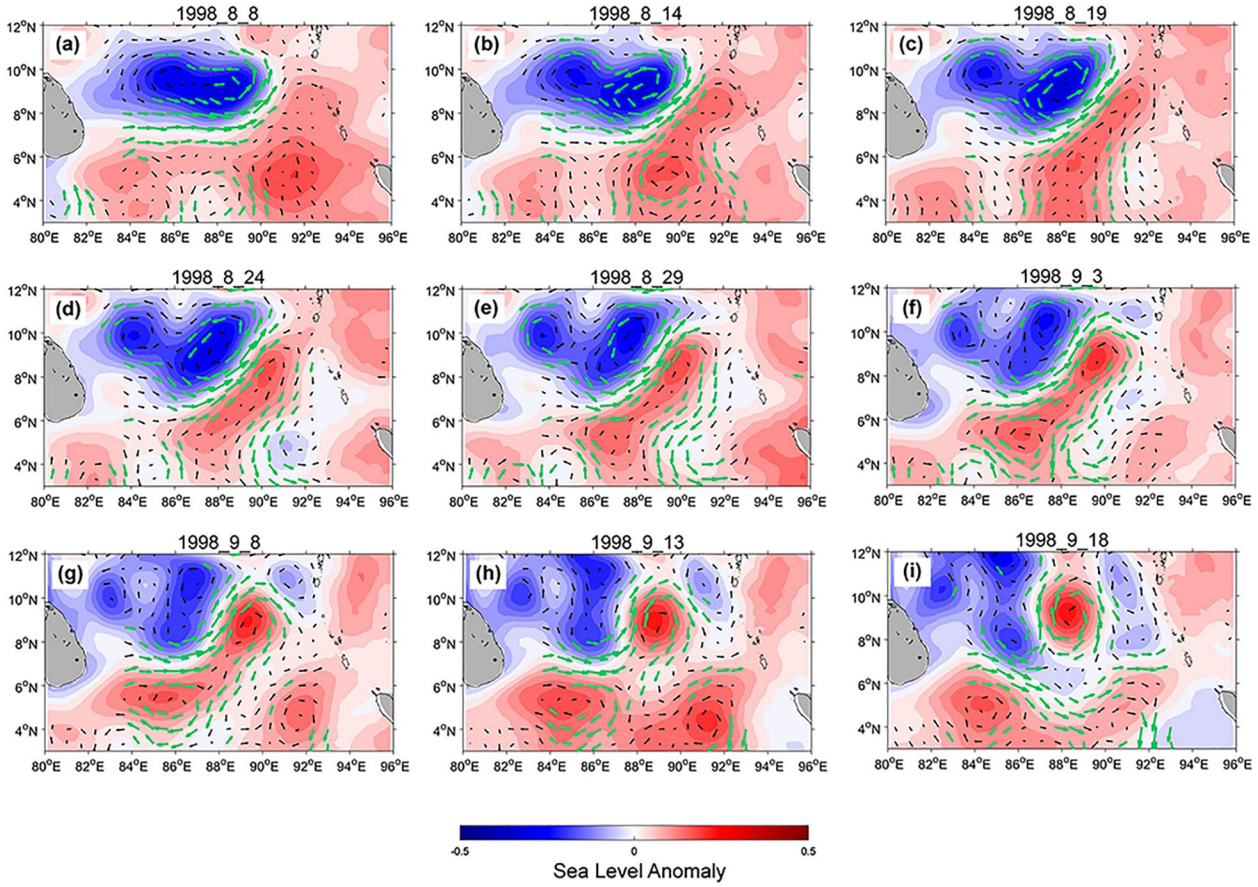

FIGURE 6
(A–I) The evolution of the sea surface currents (arrows) and sea level anomaly (color shading) from **(A)** August 8th to **(I)** September 18th, 1998. The title above each subplot indicate the date. The arrows marked in green indicate their speed exceeds 40 cm/s.

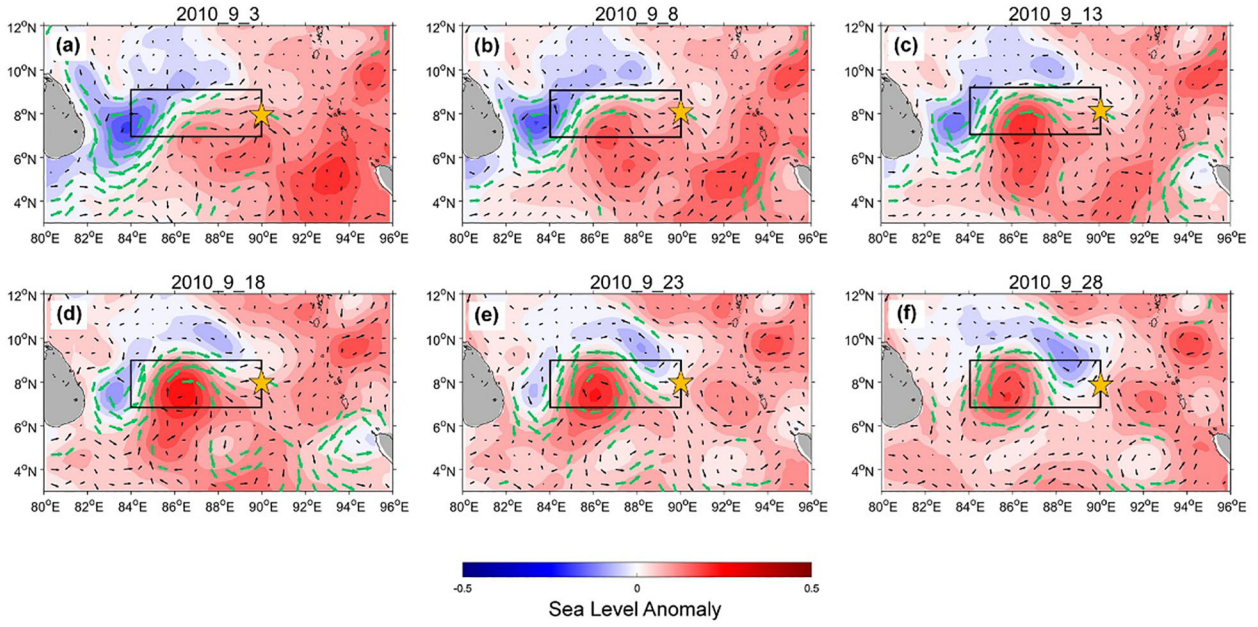

FIGURE 7
(A–F) The evolution of the sea surface currents (arrows) and sea level anomaly (color shading) from **(A)** September 3th to **(F)** September 28th, 2010. The title above each subplot indicate the date. The arrows marked in green indicate their speed exceeds 40 cm/s.

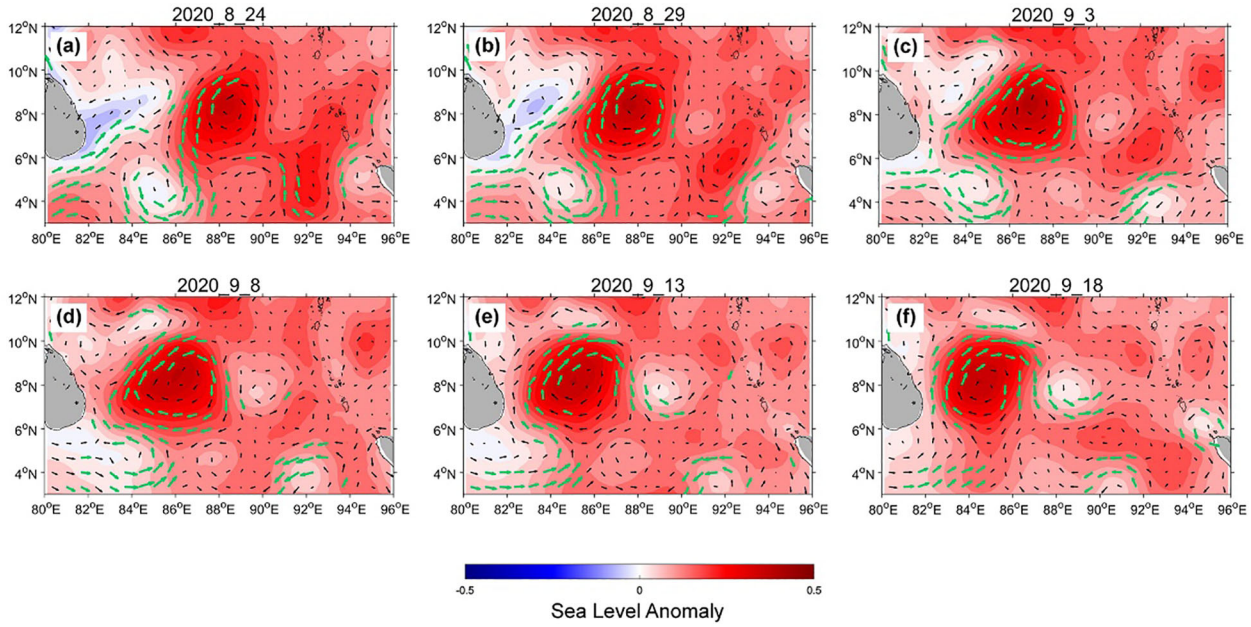

FIGURE 8
(A–F) The evolution of the sea surface currents (arrows) and sea level anomaly (color shading) from **(A)** August 24th to **(F)** September 18th, 2020. The title above each subplot indicate the date. The arrows marked in green indicate their speed exceeds 40 cm/s.

on the eastern edge of the SG eddy (as shown in Figures 6B–H, 7B–E, 8B–E). Additionally, the strengthening of recirculation/westward flow on the southern edge of the SG eddy (as shown in Figures 6G–I, 7D–F, 8C, D) leads to its eventual formation. For comparison among the years 1998, 2010 and 2020, the deformation of the SMC and the formation process of the SG eddy in 2010 are the most typical and pronounced, make it highly suitable for further instability analysis with anisotropy insight. In addition, the RAMA buoy at 90°E, 8°N, collected from 2007 to 2019 provided valuable observational data for our analysis of 2010. Therefore, the

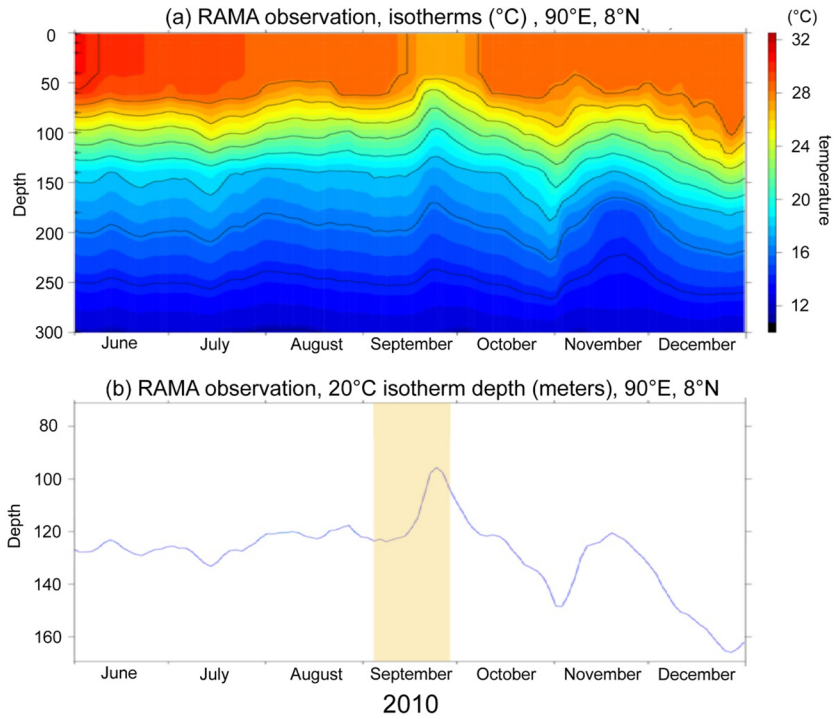

FIGURE 9
RAMA buoy observation in 90°E, 8°N. **(A)** Subsurface temperatures measured at various depths; **(B)** Depth of the 20°C isotherm.

year 2010 provides a particularly noteworthy case. The RAMA buoy observation at 90°E, 8°N in September, 2010 revealed a significant shift in the 20°C isotherm (as shown in Figure 9B). This shift indicated cold seawater below 150 meters was raised to levels shallower than 100 meters (as shown in Figure 9A). This observation confirms the presence of a negative SLA on the eastern edge of the SG eddy, which is associated with the upwelling process.

3.3 EKE budget and instability analysis with anisotropy insight

Time series of EKE budget terms averaged in upper 200 meters is shown in Figure 10A, with the 2010 SG eddy formation case highlighted in yellow. Results indicate that the direct Wind Work input into the kinetic energy field was minimal. However, the Wind Work term in EKE budget can sometimes be underestimated, as wind disturbances can indirectly diminish the stratification of the upper layer, thereby increasing instability. The contribution of the advection term is negative, signifying that EKE is transported outward to surrounding regions, corresponding to the divergence of the anticyclonic SG eddy. The BTI/T4 term directly converts kinetic energy from the mean flow field to the eddy field, the nonlinear Pressure Work term is related to disturbances in flow field and the horizontal gradient of the pressure field. Both contribute to the EKE increment.

A detailed analysis of oceanic internal instability with anisotropy insight is used to capture nonlinear processes. Thus, BTI is divided into isotropic and anisotropic components (as shown in Figure 10B), the result reveals that the isotropic component associated with flow field divergence is significantly smaller than the anisotropic component, by an order of magnitude. This confirms previous research that described the SG eddy as exhibiting weakly nonlinear planetary geostrophic divergence. The anisotropy component increases with the formation of the SG eddy and weakens rapidly thereafter, reducing the eddy's instability. This implies a self-sustaining ability to propagate westward, consistent with the argument of weak planetary wave dispersion.

Figure 10C provides further details on anisotropy, including the time series of the SG eddy's major axis inclination, the normal rate/Sn and the shear rate/Ss of the mean flow east of the SLD. Initially, cyclonic eddy-like (CE-like) negative SLA strengthened in eastern area and moved westward gradually. The southwestward current, accompanied by the CE-like SLA, increased the Ss of mean flow field in the central area of mouth region. Subsequently, the eastward flow on the northern edge of the SG eddy and the southeastward flow on the eastern edge are strengthened, explaining the continued increase in the Sn. Later, a CE-like SLA emerged at lower latitudes (near 3°N), promoting the westward recirculation on the southern edge of the SG eddy and further increasing the shear rate. Influenced by CE-like SLA signals, the SG eddy tilts its major axis towards the northeast during the initial coupling process, and returned towards the southeast after September 18th as the recirculation strengthened.

4 Summary and discussion

4.1 Summary

In this study, we revisited the anticyclonic SG eddy in the mouth region of the BOB, and analyzed the variation of oceanic internal instability with an anisotropy insight. We used LEKE to identify the signal of the anticyclonic SG eddy. Remote equatorial wind stress and local wind stress curl indices further assisted in

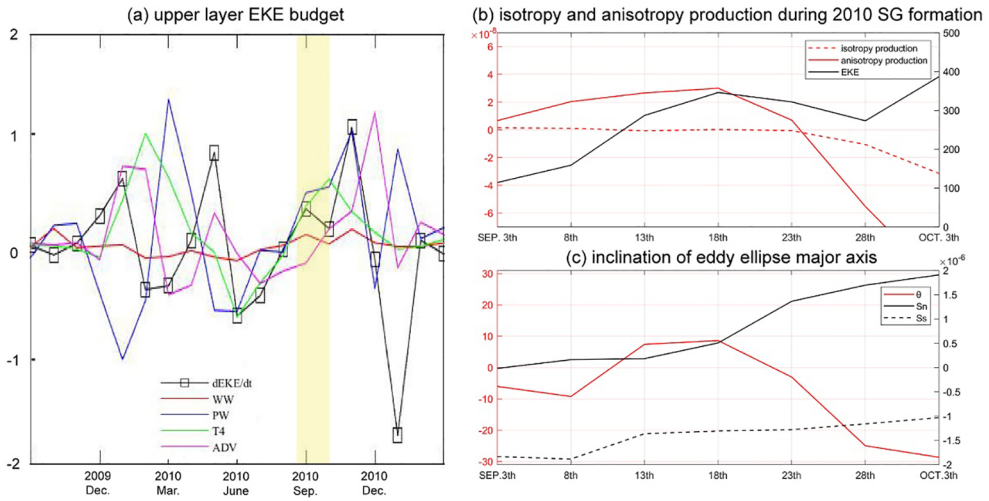

FIGURE 10
(A) Vertical-averaged EKE budget from September, 2009 to March, 2010, the SG eddy formation period is highlighted in yellow shading. **(B)** Time series of isotropic (dashed red line) and anisotropic (solid red line) components of BTI and EKE during the 2010 SG eddy formation period. **(C)** θ (red line) being the inclination of the major axis counterclockwise from the x axis, S_n and S_s are the normal (stretch) and shear rates of the mean flow strain. Results presented in figures is regional averaged, defined as SG eddy formation area (84°-90°E, 7°-9°N, indicated with black boxes in Figure 7).

identifying several typical years for further analysis: 1998, 2010, and 2020. During negative IOD years, a cyclonic anomaly developed in the surface wind field over the BOB during the SM season. Notably, both 1998 and 2010 were extreme/strong negative IOD years, while 2020 was a weak negative IOD year. In these years, the SG eddy formed as expected, with the northeastward-moving SMC on the west, and southeastward flow on the east, linked to wind stress curl-forced CE-like negative SLA signals, contributing to the SG eddy formation.

Our investigation of the oceanic internal instability during the 2010 SM season revealed that the nonlinear anisotropic component of the BTI was significantly larger than the isotropic component during SG eddy formation. Both the normal strain rate Sn and the shear strain rate Ss contributed to an increase in anisotropy. In addition, the main axis of the SG eddy initially tilted towards the northeast and then back to the southeast due to the influence of CE-like SLAs on the eastern side. Related processes mentioned above are illustrated in Figure 11. Our findings underscore the high sensitivity of anisotropic terms to currents field changes, which should be considered when further analysis of high-frequency or transient activity in the ocean is needed. As noted by Cheng et al. (2018) and Wang et al. (2022), nonlinear processes are critical for eddy generation, and anisotropic terms effectively capture certain aspects of these nonlinear processes.

4.2 Discussion

In this study, we revisited the SG eddy east of the Sri Lanka dome to improve our understanding of its complex dynamics. The year 2010 provided a comprehensive case for analyzing the formation process of the SG eddy, as shown in Figures 7, 10. Despite moderate wind field anomaly during the pre-SM season (Figure 4A), the data suggest that equatorial wind-driven waves may have contributed to the reduction of positive SLA in the eastern BOB. The significance of 2010 lies in the strong local wind stress curl anomaly over the eastern BOB during the SM season, which was the most pronounced in the 1993-2020 study period.

In addition, the RAMA buoy observations at 90°E, 8°N collected from 2007 to 2019 provided valuable data for our analysis of 2010. These observations confirmed the presence of negative SLA signals in the eastern mouth region, likely related to the upwelling process. Although our results are based on a limited number of cases and rely on observational data, they offer critical insights into the dynamics of SG eddy formation.

Figures 3, 4 are used to identity cases of the SG eddy that are primarily influenced by local wind forcing, with less influence from equatorial wind forcing. As summarized in Table 1, there were several years with strong signal of the SG eddy not significantly forced by either remote equatorial wind stress or local wind stress curl over eastern BOB, such as 2006 and 2014. This may be attributed to other mechanisms beyond the scope of this study, and we aim to elucidate these underlying mechanisms in future research.

To further explore these complex dynamics, it is essential to conduct long-term simulations to assess the broader effects of remote and local wind forcing on SG eddy formation. In future research, we plan to perform detailed ocean modelling to better quantify these effects. Once formed, the SG eddy moves westward to the east off Sri Lanka, compressing the area available for the SLD and subsequently reducing the intensity of the coastal upwelling and primary productivity in the upper ocean. Furthermore, the anticyclonic SG eddy recirculates the high-salinity seawater transported into the BOB by the SMC, potentially modulating the intensity and spatial pattern of regional circulation within the bay by changing the meridional heat flux and salinity flux.

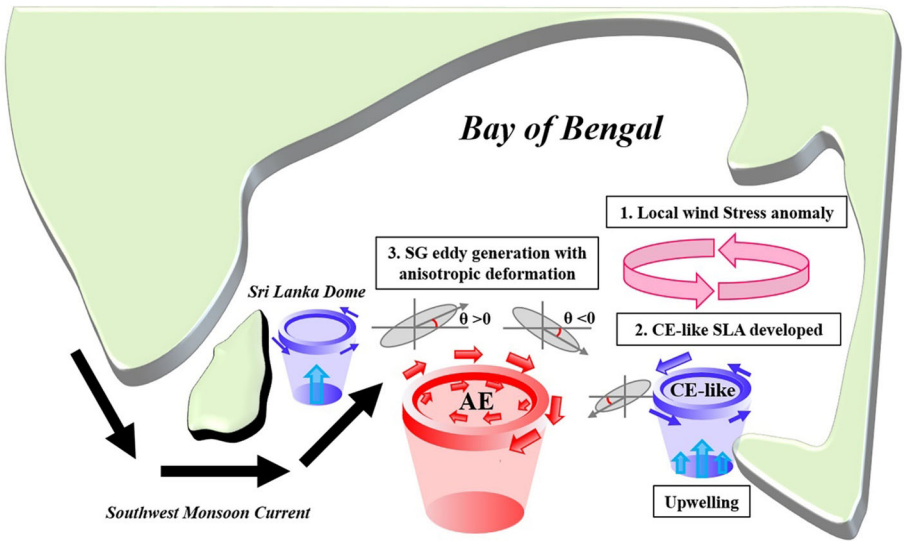

FIGURE 11
Schematic diagram. CE-like represents cyclonic eddy-like negative SLA signal, AE represents Anticyclonic eddy.

Data availability statement

The original contributions presented in the study are included in the article/supplementary material. Further inquiries can be directed to the corresponding author.

Author contributions

ZL: Conceptualization, Data curation, Investigation, Methodology, Visualization, Writing – original draft, Writing – review & editing. MS: Formal analysis, Investigation, Supervision, Writing – review & editing. PR: Investigation, Supervision, Validation, Writing – review & editing. GP: Investigation, Supervision, Validation, Writing – review & editing. DW: Conceptualization, Formal analysis, Funding acquisition, Methodology, Supervision, Writing – review & editing. WS: Investigation, Supervision, Writing – review & editing.

Funding

The author(s) declare financial support was received for the research, authorship, and/or publication of this article. This work was supported by Innovation Group Project of Southern Marine Science and Engineering Guangdong Laboratory (Zhuhai) (No. SML2023SP240) and Second Tibetan Plateau Scientific Expedition and Research (STEP) program (Grant Nos. 2019QZKK010201-02).

Conflict of interest

The authors declare that the research was conducted in the absence of any commercial or financial relationships that could be construed as a potential conflict of interest.

Generative AI statement

The author(s) declare that Generative AI was used in the creation of this manuscript. In the preparation of our research report, we have strictly adhered to the following principles: Kimi AI (https://kimi.moonshot.cn/) was utilized exclusively during the drafting phase to assist in refining sentence structures, thereby enhancing the readability and quality of the manuscript. We explicitly declare that AI was not involved in any aspect of experimental data processing or analysis. All text polished with the aid of AI technology was carried out under human supervision to ensure its accuracy and academic integrity.

Publisher's note

References

Badin, G. (2012). Surface semi-geostrophic dynamics in the ocean. *Geophysical Astrophysical Fluid Dynamics* 107 (5). doi: 10.1080/03091929.2012.740479

Beal, L. M., Vialard, J., Roxy, M. K., Li, J., Andres, M., Annamalai, H., et al. (2020). A road map to indOOS-2: better observations of the rapidly warming Indian Ocean. *Bull. Amer. Meteor. Soc* 101, E1891–E1913. doi: 10.1175/BAMS-D-19-0209.1

Burns, J. M., Subrahmanyam, B., and Murty, V. S. N. (2017). On the dynamics of the Sri Lanka dome in the bay of Bengal. *J. Geophys. Res. Oceans* 122, 7737–7750. doi: 10.1002/2017JC01298

Chen, G., Han, W., Li, Y., McPhaden, M., Chen, J., Wang, W., et al. (2017). Strong intraseasonal variability of meridional currents near 5°N in the eastern Indian Ocean: characteristics and causes. *J. Phys. Oceanogr.* 47, 979-998. doi: 10.1175/JPO-D-16-0250.1

Chen, G., Li, Y., Xie, Q., and Wang, D. (2018). Origins of eddy kinetic energy in the Bay of Bengal. *J. Geophysical Research: Oceans* 123, 2097–2115. doi: 10.1002/2017JC013455

Cheng, X., McCreary, J. P., Qiu, B., Qi, Y., Du, Y., and Chen, X. (2018). Dynamics of Eddy generation in the central Bay of Bengal. *J. Geophysical Research: Oceans* 123, 6861–6875. doi: 10.1029/2018jc014100

Cullen, K. E., and Shroyer, E. L. (2019). Seasonality and interannual variability of the Sri Lanka dome. *Deep Sea Res. Part II: Topical Stud. Oceanography* 168. doi: 10.1016/j.dsr2.2019.104642

Ding, M., Lin, P., Liu, H., Hu, A., and Liu, C. (2020). Lagrangian eddy kinetic energy of ocean mesoscale eddies and its application to the Northwestern Pacific. *Sci. Rep.* 10, 12791. doi: 10.1038/s41598-020-69503-z

Ding, R., Xuan, J., Zhou, F., Ma, X., Li, H., Huang, K., et al. (2023). Strong subsurface meridional current forced by monsoon intraseasonal oscillation in the southern Bay of Bengal during summer 2020. *Environ. Res. Lett.* 18. doi: 10.1088/1748-9326/accafd

Huang, H., Wang, D., Yang, L., and Huang, K. (2021). Enhancedintraseasonal variability of the upperlayers in the southern Bay of Bengalduring the summer 2016. *J. Geophysical Research: Oceans* 126, e2021JC017459. doi: 10.1029/2021JC017459

Ivchenko, V. O., Treguier, A. M., and Best, S. E. (1997). A kinetic energy budget and internal instabilities in the fine resolution antarctic model. *J. Phys. Oceanography* 27, 5–22. doi: 10.1175/1520-0485(1997)027<0005:AKEBAI>2.0.CO;2

Jinadasa, S. U. P., Pathirana, G., Ranasinghe, P. N., Centurioni, L., and Hormann, V. (2020). Monsoonal impact on circulation pathways in the Indian Ocean. *Acta Oceanol. Sin.* 39, 103–112. doi: 10.1007/s13131-020-1557-5

Le, Z., Huang, K., and Subrahmanyam, M. V. (2020). Energy characteristics of eddy-mean flow interaction in the estuary of Bay of Bengal in summer and autumn during 2000-2015. *Journal of Tropical Oceanography* 39 (2), 11–24. doi: CNKI:SUN:RDHY.0.2020-02-002

Pathirana, G., Chen, G., Wang, D., Abeyratne, M. K., and Priyadarshana, T. (2022). Anomalous propagation pathway of the Sri Lanka dome in summer 2014. *J. Natl. Sci. Foundation Sri Lanka*. 50 (4). doi: 10.4038/jnsfsr.v50i4.10636

Qiao, J., Qiu, C., Wang, D., Huang, Y., and Zhang, X. (2023). Multi-stage development within anisotropy insight of an anticyclone eddy in Northwestern South China Sea in 2021. *Geophysical Res. Lett.* 50, e2023GL104736. doi: 10.1029/2023GL104736

Qiu, Y., Han, W., Lin, X., West, B. J., Li, Y., Xing, W., et al. (2019). Upper ocean response to the super tropical cyclone phailin, (2013) over the freshwater region of the Bay of Bengal. *J. Phys. Oceanography* 49, 1201–1228. doi: 10.1175/JPO-D-18-0228.1

Schott, F. A., and McCreary, J. P. (2001). The monsoon circulation of the Indian Ocean. *Prog. Oceanography*. doi: 10.1016/S0079-6611(01)00083-0

Schott, F., Reppin, J., and Fischer, J. (1994). Currents and transports of the monsoon current south of Sri Lanka. *J. Geophys. Res.* 99, 25 127–25 141. doi: 10.1029/94JC02216

Vinayachandran, P. N., and Yamagata, T. (1998). Monsoon response of the sea around Sri Lanka: generation of thermal domes and anticyclonic vortices. *J. Phys. Oceanogr.* 28, 1946–1960. doi: 10.1175/1520-0485(1998)028<1946:MROTSA>2.0.CO;2

Wang, X., Cheng, X., Liu, X., and Chen, D. (2021). Dynamics of eddy generation in the southeast tropical Indian Ocean. *J. Geophysical Research: Oceans* 126, e2020JC016858. doi: 10.1029/2020JC016858

Waterman, S., and Lilly, J. M. (2015). Geometric decomposition of eddy feedbacks in barotropic systems. *J. Phys. Oceanography* 45, 1009–1024. doi: 10.1175/JPO-D-14-0177.1

Williams, G. P., and Yamagata, T. (1984). Geostrophic regimes, intermediate solitary vortices and Jovian eddies. *J. Atmos. Sci.* 41, 453–478. doi: 10.1175/1520-0469(1984)041<0453:GRISVA>2.0.CO;2

Wyrtki, K. (1973). An equatorial jet in the Indian Ocean. *Science* 181, 262–264. doi: 10.1126/science.181.4096.262

Yamagata, T. (1982). On nonlinear planetary waves: A class of solutions missed by the traditional quasi-geostrophic approximation. *J. Oceanogr. Soc Japan* 38, 236–244. doi: 10.1007/BF02111106

Zu, T., Yan, C., Belkin, I., Zhuang, W., and Chen, J. (2013). Evolution of an anticyclonic eddy southwest of Taiwan. *Ocean Dynamics* 63, 519–531. doi: 10.1007/s10236-013-0612-6